Scaling Up Pullulan-Based Supercapacitors: A Sustainable Approach to Binder and Separator Integration in EDLCs

Elisabetta Petri[1,2], Maria Arnaiz[3], Chiara Gualandi[1,4,5], Francesca Soavi[1,2,4,*], Jon Ajuria[3,*]

[1]*Department of Chemistry "Giacomo Ciamician", Alma Mater Studiorum University of Bologna Via Piero Gobetti, 85-40129 Bologna, Italy*
[2]*Center for the Environment, Energy, and Sea - Interdepartmental Centre for Industrial Research in Renewable Resources, Environment, Sea and Energy (CIRI-FRAME), Alma Mater Studiorum University of Bologna Viale Ciro Menotti, 48 - 48122 Marina di Ravenna (RA), Italy*
[3]*Centre for Cooperative Research on Alternative Energies (CIC energiGUNE), Basque Research and Technology Alliance (BRTA), Alava Technology Park, Albert Einstein 48, 01510 Vitoria-Gasteiz, Spain*
[4]*National Reference Center for Electrochemical Energy Storage (GISEL) - INSTM UdR of Bologna, Via G. Giusti 9, 50121, Firenze, Italy*
[5]*Interdepartmental Center for Industrial Research on Advanced Applications in Mechanical Engineering and Materials Technology, CIRI-MAM, University of Bologna, Viale Risorgimento, 2, 40136 Bologna, Italy*

*Corresponding authors: francesca.soavi@unibo.it, jajuria@cicenergigune.com

Keywords: supercapacitors; pullulan; electrospun separators; water processable electrodes and separator; biopolymer

Supplementary Information

Figure S1 illustrates typical Nyquist plots for EDLCs, comparing an ideal case (Figure S1a) with not fully optimized devices (i.e., lab cells) (Figure S1b). In the high-frequency region, the resistance is predominantly influenced by the ionic conductivity of the electrolyte. Two main features define the resistance in this region: (i) the series resistance (R_s), represented by the intercept with the real axis, and (ii) the resistance associated with the electrode pores (R_p), which is usually negligible in well-optimized systems like industrial supercapacitors. Rs is affected by factors such as electronic contact resistance, gaps between the electrode material and current collector and the carbon structure, and electrolyte ionic resistance [1]. R_s corresponds to the equivalent series resistance (ESR), which can be determined from the ohmic drop observed in GCPL analysis. On the other hand, R_p is influenced by inter-granular electronic and ionic resistance, the material–current collector interface resistance, and any passive coatings that may develop on the current collector surface. R_p is in parallel with a constant phase element (Q) that describes the capacitance related to the electrode's external surface. In the plot, R_p and Q give rise to a high-frequency semicircle, with a diameter that corresponds to R_p. At medium frequencies, the in-pore resistance (R_{INP}) reflects the resistance faced by the electrolyte as it penetrates the electrode pores [2]. This is complex and modelled using a transmission line described by the Warburg impedance element in equivalent circuit models (W) [3]. Finally, the low-frequency region of the Nyquist plot deviates from the linear trend, parallel to the y-axis, expected for ideal EDLCs. In ideal EDLCs, the imaginary component of the impedance is related to the EDLC capacitance. The deviation from the ideal behaviour is related to the pore size distribution resistance (R_{PSD}), which is determined by the accessibility of the pores to the ions [4]. The total cell resistance (EDR) is the cumulative result of these resistive phenomena across all frequency ranges.

Thus, the EDLC behaviour can be modelled by equivalent series circuits, and the resulting Nyquist plot is reported in Figure S1b. As an example, Figure S1c reports the Nyquist plots of S-sPUL-AC70 and the equivalent electrical circuit (ECC) used to fit the data.

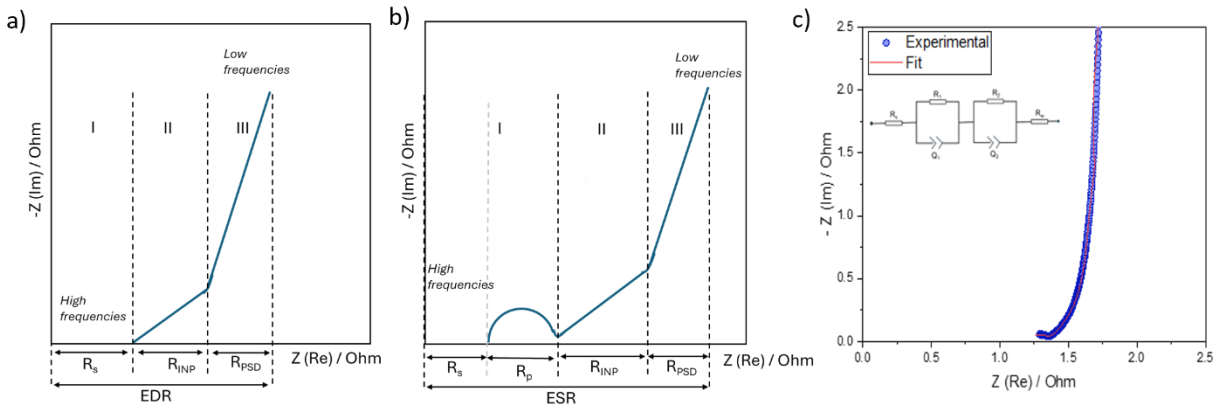

Figure S1. Nyquist plot of (a) ideal and (b) real EDLC divided by frequency region and influence parameters, and Nyquist plot of (c) S-sPUL-AC70 with the corresponding equivalent circuit and fitting.

Table S1. EDLCs specific capacitance referred to the total electrode mass, evaluated by the galvanostatic voltage discharge profile at different specific currents.

	S-sPUL-AC70	***S-sPUL-AC88***	***S-sPUL-AC91***
Spec. Current ***($A\ g^{-1}$)***	***Spec. Capacitance*** ***($F\ g^{-1}$)***	***Spec. Capacitance*** ***($F\ g^{-1}$)***	***Spec. Capacitance*** ***($F\ g^{-1}$)***
0.25	19.8	22.2	19.7
0.5	19.7	22.0	19.2
1	19.5	21.7	18.7
2	19.4	21.4	18.3
3	19.3	21.3	18.2
5	19.3	21.1	18.0
7	19.2	20.9	17.9
10	19.2	20.8	17.7

Table S2. EDLCs specific power and specific energy referred to the total electrode mass, evaluated by the galvanostatic voltage discharge profile at different specific currents.

	S-sPUL-AC70		***S-sPUL-AC88***		***S-sPUL-AC91***	
Spec. Current ***($A\ g^{-1}$)***	***Spec.Power*** ***($kW\ kg^{-1}$)***	***Spec.Energy*** ***($Wh\ kg^{-1}$)***	***Spec. Power*** ***($kW\ kg^{-1}$)***	***Spec.Energy*** ***($Wh\ kg^{-1}$)***	***Spec.Power*** ***($kW\ kg^{-1}$)***	***Spec.Energy*** ***($Wh\ kg^{-1}$)***
0.25	0.2	20.0	0.3	22.4	0.3	19.9
0.5	0.5	19.8	0.7	22.1	0.7	19.3
1	0.9	19.6	1.3	21.7	1.3	18.7
2	1.9	19.3	2.7	21.3	2.6	18.2
3	2.8	19.1	4.0	21.0	3.9	17.9
5	4.6	18.7	6.6	20.4	6.5	17.5
7	6.4	18.3	9.2	20.0	9.0	17.1
10	9.0	17.9	12.9	19.4	12.8	16.5

To qualitatively evaluate the thermal stability of the electrospun pullulan (PUL) membrane, a stepwise heating test was performed. A square membrane sample of 2x2 cm was placed on a hot plate and gradually heated from room temperature (RT) to 250 °C under ambient atmosphere. The temperature was increased in steps of 10 °C, and the membrane was held at each temperature for 2 minutes before proceeding to the next temperature. At each step, the sample was monitored by any changes in morphology, color, dimensional stability, or mechanical integrity. Figure S2, shows that the electrospun PUL membrane maintains its shape and white color throughout the entire heating process. No significant shrinkage and deformation were observed.

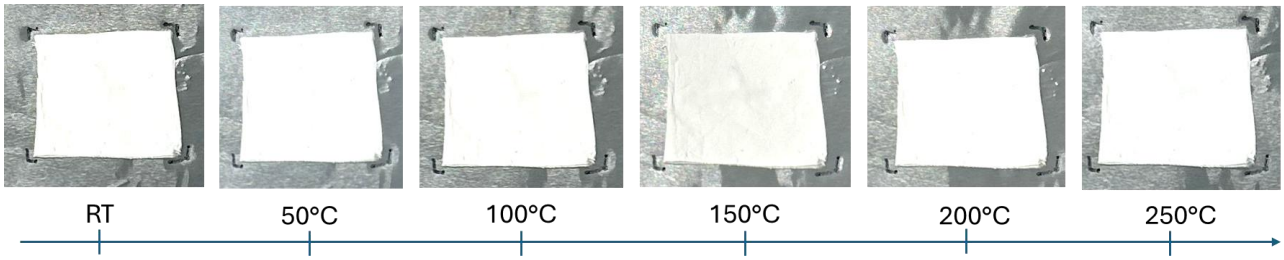

Figure S2. Thermal stability test of the electrospun PUL membrane by heating from room temperature to 250 °C on a hot plate. The membrane was heated on a hot plate from room temperature to 250 °C, with 2-minute holds at each temperature step.

Tensile stress-strain tests were carried out using an Instron 4465 (Instron, USA) tensile testing machine on rectangular samples cut from the PUL membranes (gauge length = 20 mm, width = 5 mm, thickness = 0.08-0.12 mm) subjected to uniaxial deformation with a rate of 10 mm min^{-1}. Mechanical data such as Young's modulus, strain at break, and stress at break were determined from the resulting stress-strain curves. Four samples per composition were tested, and results were provided as the average value ± standard deviation.

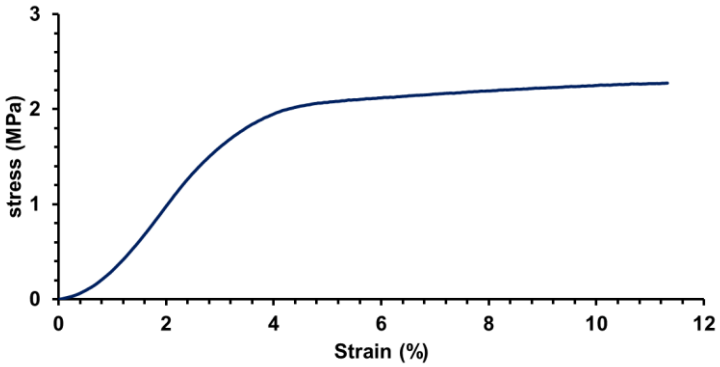

Figure S3. Representative stress-strain curve from uniaxial tensile testing of PUL electrospun membrane. Young's modulus = 71 ± 5 MPa; stress at break = 2 ± 0.2 MPa; deformation at break = 10 ± 2 %.

Static contact angle measurements were performed on electrospun PUL membrane by using the optical tensiometer Attension Theta Lite (Biolin Scientific) under ambient conditions by recording the side profiles of electrolyte drops. Two electrolytes were tested: 1 M Et_4NBF_4 - acetonitrile and 1 M Et_4NBF_4 - propylene carbonate. The shape of the drop was recorded in a time range of 0 - 10 s at 26 frames per seconds. At least four drops were observed for each electrolyte.

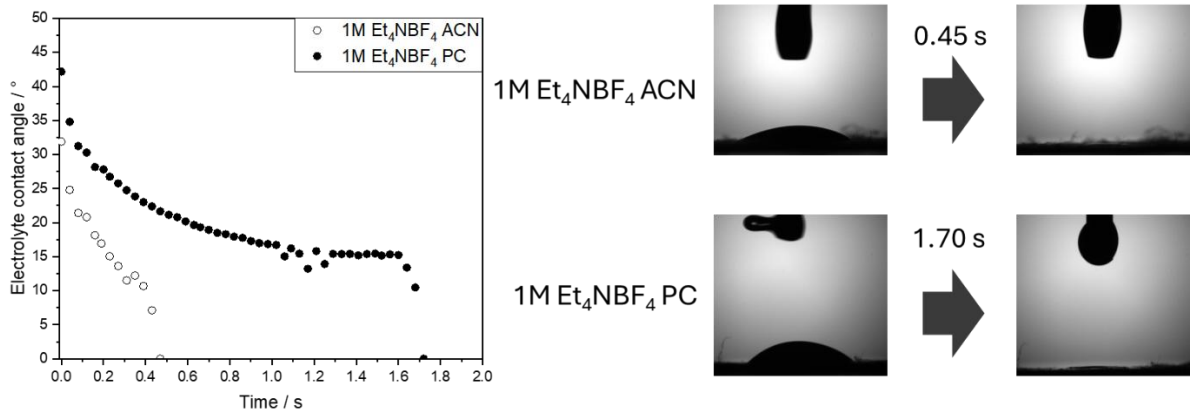

Figure S4. (a) Contact angle behavior over time of Pullulan fibers wet with a drop of 1M Et_4NBF_4-ACN and 1M Et_4NBF_4-PC. (b) Shape of electrolyte droplets on the electrospun mats and their evolution with time.

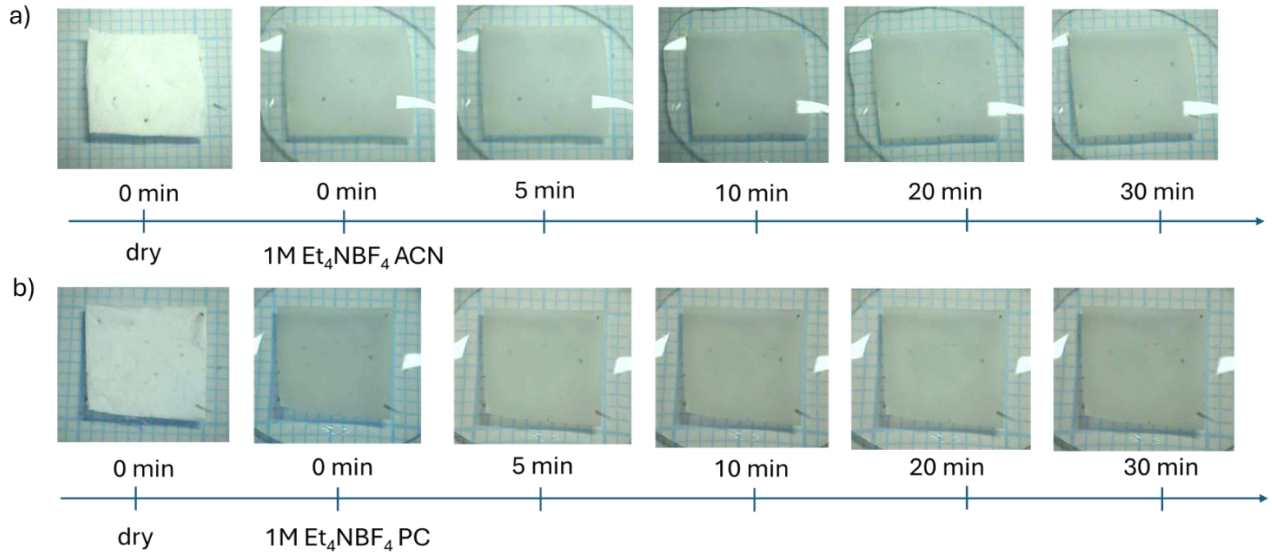

Figure S5. Electrospun PUL/membrane in its dry state and after impregnation with the two electrolytes (1M Et_4NBF_4 ACN and 1M Et_4NBF_4 PC) over time.

Table S3. Pouch cells code, EDLCs mass and mass loading, considering the total electrode mass of the PUL-based cells tested with different electrolytes and with PUL membrane separator.

Pouch cell code	***EDLCs Mass (mg)***	***EDLCs Mass loading (mg cm^{-2})***	***Electrolyte***
P-dPUL-ACN	187.0	9.4	1 M Et_4NBF_4 ACN
P-dPUL-PC	179.2	9.0	1 M Et_4NBF_4 PC

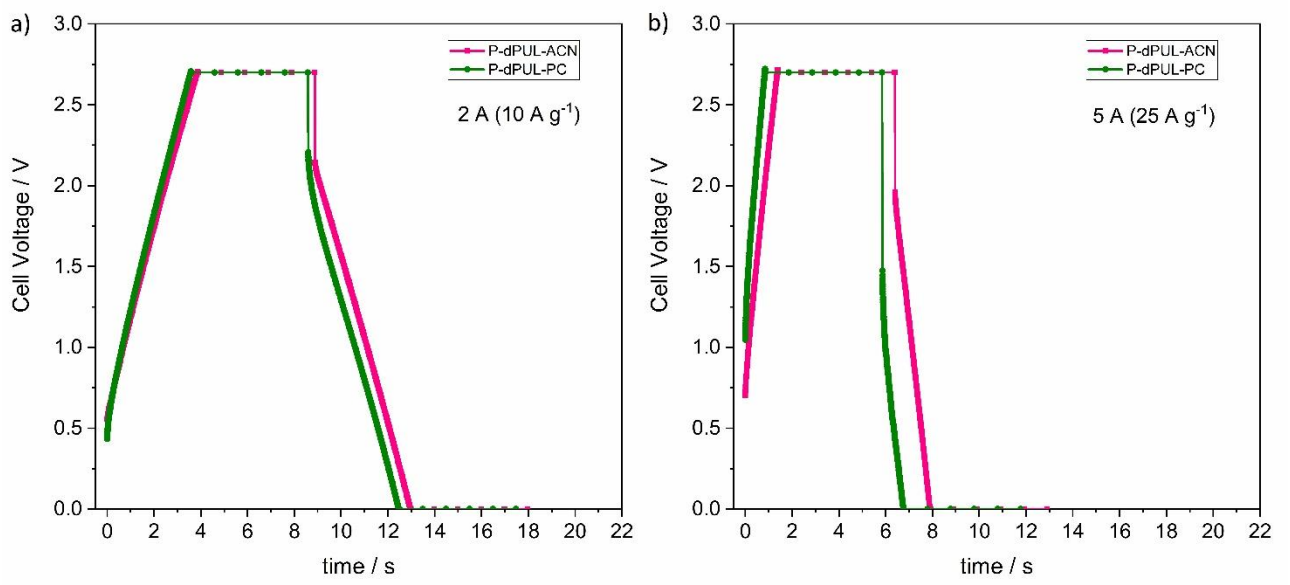

Figure S6. GCPL charge/discharge profiles at (a) 2 A (10 A g^{-1}) and (b) 5 A (25 A g^{-1}) at RT of the pouch cells with PUL-electrodes, PUL-separator and ACN or PC-based electrolyte.

Table S4. Specific capacitance of pouch cells with dPUL-AC88 electrodes and with 1M Et_4NBF_4 ACN and 1M Et_4NBF_4 PC referred to the total electrode mass, evaluated by the galvanostatic voltage discharge profile at different specific currents.

		P-dPUL-ACN	***P-sPUL-PC***
Current (A)	***Spec. Current ($A\ g^{-1}$)***	***Spec. Capacitance ($F\ g^{-1}$)***	***Spec. Capacitance ($F\ g^{-1}$)***
0.1	0.5	20.8	21.1
0.2	1.0	20.6	20.9
0.5	2.5	20.4	20.5
1	5.0	20.3	20.2
2	10.0	20.4	19.6
3	15.0	20.6	18.9
5	25.0	20.6	17.2
10	50.0	19.9	6.7

Table S5. The specific capacitance, energy and power values from GCPL at different currents, delivered by the EDLCs assembled with AC:PUL-Gly:C45 (88:8:4) electrodes and PUL membrane separator and 1M Et_4NBF_4 ACN and 1M Et_4NBF_4 PC.

Pouch Cell code	***EDLCs Mass loading$_{electrode}$ (mg cm^{-2})***	***Spec.Capacitance (F g^{-1})***	***Spec. Power (kW kg^{-1})***	***Spec. Energy (Wh kg^{-1})***
P-dPUL-ACN	9.4	20.8 (0.1 A) 20.3 (1 A) 20.6 (5 A)	0.7 (0.1 A) 6.1 (1 A) 26.2 (5 A)	20.3 (0.1 A) 14.7 (1 A) 10.9 (5 A)
P-dPUL-PC	9.0	21.1 (0.1 A) 20.2 (1 A) 17.2(5 A)	0.7 (0.1 A) 6.8 (1 A) 20.6 (5 A)	20.9 (0.1 A) 16.8 (1 A) 5.2 (5 A)

References

[1] T.S. Mathis, N. Kurra, X. Wang, D. Pinto, P. Simon, Y. Gogotsi, Energy Storage Data Reporting in Perspective—Guidelines for Interpreting the Performance of Electrochemical Energy Storage Systems, Adv Energy Mater 9 (2019). https://doi.org/10.1002/AENM.201902007.

[2] R. de Levie, On porous electrodes in electrolyte solutions. I. Capacitance effects, Electrochim Acta 8 (1963) 751–780. https://doi.org/10.1016/0013-4686(63)80042-0.

[3] A.A. Moya, Low-frequency approximations to the finite-length Warburg diffusion impedance: The reflexive case, J Energy Storage 97 (2024) 112911. https://doi.org/10.1016/J.EST.2024.112911.

[4] H.K. Song, H.Y. Hwang, K.H. Lee, L.H. Dao, The effect of pore size distribution on the frequency dispersion of porous electrodes, Electrochim Acta 45 (2000) 2241–2257. https://doi.org/10.1016/S0013-4686(99)00436-3.